*Macedonian Journal of Chemistry and Chemical Engineering*, Vol. **34**, No. 2, pp. 351–362 (2015)

MJCCA9 – 693

ISSN 1857-5552
e-ISSN 1857-5625

Received: November 6, 2014

UDC: 615.373.074:543.422.3-74
615.373.074:543.424.2

Accepted: December 10, 2014

*Original scientific paper*

# EVALUATION OF NON-RADIOACTIVE LUTETIUM- AND YTTRIUM-LABELED IMMUNOCONJUGATES OF RITUXIMAB – A VIBRATIONAL SPECTROSCOPY STUDY

**Darinka Gjorgieva Ackova[1,*], Katarina Smilkov[1], Emilija Janevik-Ivanovska[1], Trajče Stafilov[2], Zorica Arsova-Sarafinovska[1,3], Petre Makreski[2,*]**

[1]*Faculty of Medical Sciences, Goce Delčev University, 2000 Štip, Republic of Macedonia*
[2]*Institute of Chemistry, Faculty of Natural Sciences and Mathematics, Ss. Cyril and Methodius University, 1000 Skopje, Republic of Macedonia*
[3]*Institute of Public Health of the Republic of Macedonia, Centre of Reference Laboratories, 1000 Skopje, Republic of Macedonia*

petremak@pmf.ukim.mk; darinka.gorgieva@ugd.edu.mk

Fourier Transform Infrared (FT-IR) and Raman spectroscopy were used to study the molecular structure of the recombinant monoclonal antibody and anti-CD20-conjugates which are intended to be used as anti-cancer therapeutic agents. We characterized the secondary structure of a therapeutic immunoconjugate of rituximab, formulated with three different bifunctional chelating agents (*p*-SCN-Bn-DOTA, *p*-SCN-Bn-DTPA, and 1B4M-DTPA) and labeled with non-radioactive lutetium and yttrium. The secondary structure content of all three immunoconjugates was assessed to be similar to that of unlabeled antibody. In addition, no significant changes upon lyophilizing procedures were observed. The results demonstrate that amide bands could be used as analytical tool which provides a quick and reliable way for screening of protein pharmaceuticals during the development of lyophilized formulations.

**Keywords:** rituximab; bifunctional chelating agents; FT-IR; Raman spectroscopy

## ЕВАЛУАЦИЈА НА ИМУНОКОНЈУГАТИ НА РИТУКСИМАБ ОБЕЛЕЖАНИ СО НЕРАДИОАКТИВНИ ЛУТЕЦИУМ И ИТРИУМ – СТУДИЈА СО ВИБРАЦИОНА СПЕКТРОСКОПИЈА

За испитување на молекулската структура на рекомбинантно моноклонално антитело и анти-CD20-конјугати наменети за употреба како антиканцерни терапевтски агенси е користена инфрацрвена (ИЦ) и раманска спектроскопија. Секундарната структура на терапевтски имуноконјугат на ритуксимаб е карактеризирана во негови формулации со три различни бифункционални хелирачки агенси (*p*-SCN-Bn-DOTA, *p*-SCN-Bn-DTPA, 1B4M-DTPA) обележани со нерадиоактивни лутециум и итриум. Најдено е дека секундарната структура на сите три типа имуноконјугати е слична со таа на необележаното антитело. Освен тоа, не беа забележани значајни промени после процесот на лиофилизација на имуноконјугатите. Добиените резултати покажаа дека амидните вибрациони ленти можат да бидат искористени како аналитичка алатка која овозможува брз и веродостоен начин за скрининг на протеински лекови во текот на процесот на развој на лиофилизирани формулации.

**Клучни зборови:** ритуксимаб; бифункционални хелирачки агенси; инфрацрвена и раманска спектроскопија

## 1. INTRODUCTION

Monoclonal antibodies are among the main categories of molecules used in targeted therapy. In radioimmunotherapy, monoclonal antibodies (mAbs) are attached to a therapeutic radioisotope, where these antibodies act as a carrier and target tumor cells [1]. An inherently radiosensitive malignancy, known as Non-Hodgkin's lymphoma (NHL), has provided the basis for radioimmunotherapy. CD20 receptor has proven to be an excellent target for the treatment of B-cell lymphoma [2]. More than 90% of B-cell lymphoma cells express CD20, but it is not promoted on cells in stem and progenitor cell pools. Rituximab (Rituxan™, Genentech Inc., South San Francisco, CA, and Biogen-IDEC Pharmaceutical Corp, San Diego, CA), a mouse-human chimeric mAb produced in CHO cells that reacts with CD20, has proven to be highly effective and relatively non-toxic in the treatment of B-cell malignancies [3, 4]. Until now, two anti-CD mAb products have been approved in the United States for the treatment of B-cell lymphomas: the radiolabeled antibodies Y-90 ibritumomab tiuxetan (Zevalin™, Biogen-IDEC Pharmaceuticals, San Diego, CA) and I-131 tositumomab (Bexxar™, GlaxoSmithKline, Research Triangle Park, NC) [5, 6]. Radioimmunotherapy is found to be more advantageous compared to unlabeled therapeutic antibodies, given the additive effect of radiation-induced cytotoxicity and the ability of the associated radioactivity to kill the adjoining cancerous tumor cells that may not have bound the radiolabeled antibody [7].

The success in application of rituximab is highly dependent on the physical and chemical properties of the radioisotope attached. Among the various radionuclides, radiolanthanides are of particular interest and several isotopes are available: the low energy β-emitter $^{177}$Lu, medium energy β-emitters ($^{153}$Sm), and the high energy β-emitter $^{166}$Ho. Depending on the tumor size and location, the choice of β-emitter may be different [8]. For systemic cancer radiotherapy, $^{90}$Y is of particular interest due to its high-energy pure β-particle emission. $^{90}$Y has a half-life of 2.7 days, which is short enough to achieve a critical dose rate and, at the same time, durable enough to allow the manufacture, transportation and delivery of the radiopharmaceutical for clinical use. The specific activity for $^{90}$Y is very high, and is well suited for the development of receptor-based therapeutic radiopharmaceuticals [9]. $^{177}$Lu is a β- and γ-emitter radionuclide (half-life 6.65 days) whose short-range β-particles (0.04–1.8 mm) with low energy (0.497 MeV, 78.7% abundance) are suitable for therapeutic purposes. Moreover, the main γ-photons of $^{177}$Lu (0.208 MeV, 11% abundance) are appropriate for gamma imaging and can be used for dosimetric estimations in humans. Due to its proper characteristics, $^{177}$Lu is being increasingly used in research studies [10–13]. Over the years, a number of chelating agents have also been investigated for labeling proteins and peptides with radioisotopes. The most widely investigated agents are various derivatives of the acyclic agent diethylene triamine pentaacetic acid (DTPA) and the macrocyclic agent 1,4,7,10-tetraazacyclododecane-1,4,7,10-tetraacetic acid (DOTA) [14]. In some of these investigations, the labeling of antibodies and their fragments with $^{177}$Lu has been achieved using 2-(4-isothioyanatobenzyl)diethylenetriaminepentaacetic acid (*p*-SCN-Bn-DTPA), cyclic DTPA dianhydride and 1,4,7,10-tetraaza-N-(1-carboxy-3-(4-nitrophenyl)propyl)-*N′*, *N″*,*N‴*-tris(acetic acid) cyclododecane (PA-DOTA) [10–12, 15–18]. Although the preparations of these and other derivatives of DOTA and DTPA radioimmunoconjugates have been reported [11, 12, 14], chemical characteristics, stability and the biodistribution of the prepared radioimmunoconjugates have not been examined in detail.

Therapeutic monoclonal antibodies are very complex molecular structures that are joined together with weak, non-covalent or strong covalent disulfide bonds. Keeping the bonding integrity is of utmost importance for the physicochemical stability and immunological potential. Therapeutic proteins are usually formulated in aqueous solution to allow ease of use, but it is also known that an aqueous environment can accelerate many degradation processes [19, 20]. The common approach to the stabilization of therapeutic proteins is lyophilization, which is a reliable process that can assure the product sterility requirements without the stress of thermal sterilization [21].

In order to obtain $^{90}$Y- and $^{177}$Lu-anti-CD20 radioimmunoconjugates for using in diagnostic/therapeutic studies, different bifunctional chelating agents-anti-CD20 (rituximab) (BFCA-rituximab) were labeled with non-radioactive Y and Lu for preliminary physicochemical characterization. This work aims to examine ready-to-label lyophilized rituximab immunoconjugates with different BFCAs, 2-(4-isothiocyanatobenzyl)-1,4,7,10 tetraazacyclododecane-tetraacetic acid (*p*-SCN-Bn-DOTA), 2-(4-isothiocyanatobenzyl) diethylenetriamine-pentaacetic acid (*p*-SCN-Bn-DTPA) and 2-(4-isothiocyanatobenzyl)-6-methyl-diethylene-triaminepentaacetic acid (1B4M-DTPA) by infrared (IR) and Raman spectroscopy to reveal the possible post-conjugation, post-lyophilization and post-

labeling modifications. The main goal was to determine the suitability of preparation and labeling procedures to obtain kit formulations ready for radioactive labeling. In fact, we examined the possibility to assess some relevant structural elements of the immunoconjugates by FT-IR and Raman spectroscopy "fingerprint" techniques.

## 2. MATERIALS AND METHODS

### 2.1. *Materials*

All three conjugation agents with ≥94% purity were obtained from Macrocyclics Inc. (NJ, USA). Rituximab was purified from a commercial sample (Mabthera®), purchased from Roche Co, CA, USA, using ultrafiltration (Ultracel® – 30K, Millipore, Ireland) for concentration and buffer exchange to sterile 0.1 M PBS, pH 8.0.

### 2.2. *Conjugation of rituximab to three different BFCAs*

BFCAs were dissolved in 0.1 M PBS (pH 8.0) to a concentration of 10 mg/ml. Calculated amounts of BFCA required to give a 20-fold molar excess over the amount of rituximab (10 mg/ml) were added to the antibody solution. The mixtures were incubated at 4 °C overnight with gentle shaking. Purification was performed by rinsing the immunoconjugates with 0.05 M ammonium acetate (pH 7.0), in ultrafiltration devices (Ultracel®), until absorbance in the ultrafiltrate, set at 280 nm, was nearly zero. The concentrations were adjusted to 1 mg/ml and solutions were lyophilized to solid state.

### 2.3. *Lyophilization process*

The lyophilization was performed by using Labconco Free Zone Stoppering Tray Dryer (USA), modifying the protocol described by Park et al. [22] as follows. The solutions of immunoconjugates were transferred to 10 ml (type I glass) tubing vials using a fill volume of 1 ml. The vials were partially covered with suitable stoppers and equally distributed on the shelves of the apparatus. In order to monitor the temperature variations, thermocouples were placed in the center of each shelf using a blank vial. The samples were loaded at shelf temperature of 5 °C. The temperature was then decreased to –40 °C at a rate of 0.40 °C/min and held for 3 h. An annealing step was included, at –15 °C, to allow complete crystallization, thus completing the freezing step in 10 h. The primary drying was performed at –10 °C for 25 h. The secondary drying was performed at the shelf temperature of 25 °C for 11 h. Upon completion of the process, the vials were covered and kept at 4 °C until analysis.

### 2.4. *Labelling the BFCA-rituximab conjugates with non-radioactive Lu and Y*

BFCA-rituximab conjugates in the form of freeze-dried preparations were dissolved with sterile saline, and subsequently labeled with 1.0709 μg $LuCl_3$ [equivalent to maximum tolerated dose (MTD) for $^{177}$Lu (118.3 mCi)] or with 1.1555 mg $YCl_3$ [equivalent to MTD for $^{90}$Y (28.37 mCi)] in a total volume of 1 ml at pH 7.0, before being incubated for 30 min at room temperature (*p*-SCN-Bn-DTPA-rituximab and 1B4M-DTPA-rituximab) and 60 min at 40 °C (*p*-SCN-Bn-DOTA-rituximab).

### 2.5. *FT-IR and Raman spectroscopy*

FT-IR and Raman spectroscopy were applied for determination of protein secondary structure. FT-IR spectroscopy measurements were conducted on PARAGON 1000 (Perkin Elmer) spectrophotometer in the spectral range 2000–500 $cm^{-1}$ and the plates were scanned three times to minimize the influence of spotting variance. Attenuated Total Reflectance (ATR) spectra were acquired at a resolution of 4 $cm^{-1}$ and 128 spectra were accumulated in order to improve the signal-to-noise ratio. After spectral acquisition, data manipulation was performed with the Grams_32 software (Thermo Scientific).

The room temperature Raman spectra (2000–400 $cm^{-1}$) were recorded on a micro-Raman multichannel spectrometer Horiba JobinYvon LabRam 300 Infinity. The Raman effect was obtained using 632.8 nm line from a He:Ne laser. An Olympus MPlanN confocal microscope with ×100 objective for magnification was selected. The spectral resolution was set to 4 $cm^{-1}$. In order to focus the laser beam, a confocal hole of about 2 μm was used and the position on the sample surface was adjusted by using a motorized *x-y* stage. The Raman shift was calibrated by using the Raman peak of silica located at 520.7 $cm^{-1}$. The acquisition time and the accumulation number were set to 10 s and 10 scans, respectively.

## 3. RESULTS AND DISCUSSION

Structural and orientation changes are often a part of protein interactions due to various factors such as specific/nonspecific attachment, hydration/dehydration, and experimental conditions [23]. In order to assess the stability of monoclonal anti-

bodies, this study was aimed at monitoring the changes in physicochemical properties of rituximab conjugates after lyophilization and non-radioactive labeling. The structural formulae of BFCAs used for conjugation of the antibody are shown in Figure 1.

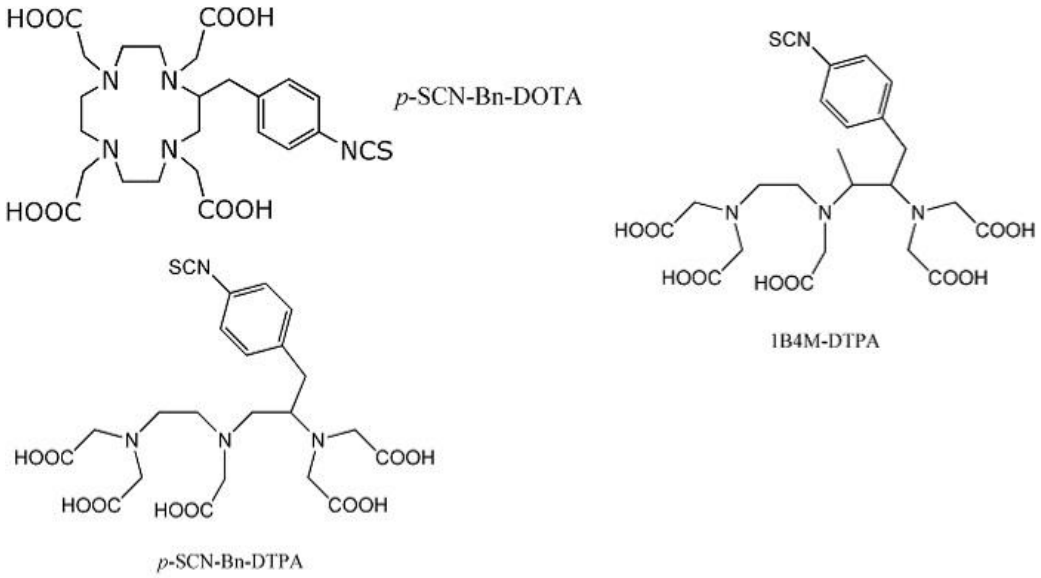


**Fig. 1.** Structural formulae of BFCAs used for conjugation

To obtain evidence for preserved secondary antibody structure (which is mandatory for therapeutic immunoconjugates) and possible post-non-radioactive labelling modifications, a vibrational spectroscopic study was performed. Protein denaturation upon lyophilization is usually monitored by IR spectroscopy [24], although other methods such as mass spectroscopy [25], and Raman spectroscopy [26] are also applied. In this study, IR and Raman spectroscopy were used for extensive characterization of the immunoconjugates of interest by monitoring molecular vibrations of the structural building units.

IR and Raman spectroscopic applications for protein pharmaceuticals (in their native and denatured state) include evaluation of the conformation changes, protein–protein interactions, protein aggregation and protein–drug product characterization. Vibrational spectra can be used to estimate the secondary structure of proteins by inspection of the frequencies at which the amide bonds absorb infrared radiation (Table 1) [27–30].

The experimental IR spectra (in the region 2000–500 $cm^{-1}$) of investigated compounds are displayed in Figure 2 and Figure 3, whereas the band assignment is given in Table 2. On the other hand, the obtained Raman spectra (2000–400 $cm^{-1}$ region) of unlabeled and non-radioactively labeled immunoconjugates are presented in Figure 4 and Figure 5, with the corresponding band assignments listed in Table 3.

T a b l e 1

*Characteristic vibrational bands for the secondary structure of proteins (according to Ref. [29] and [30])*

| Designation and description | Approximate frequency ($cm^{-1}$) |
|---|---|
| Amide I (C=O stretching) | 1600–1690 |
| Conformation determining band position: | |
| α-helix | 1650–1657 |
| Antiparallel β-sheet | 1612–1640; 1670–1690 (weak) |
| Parallel β-sheet | 1626–1640 |
| Turn | 1655–1675; 1680–1696 |
| Unordered | 1640–1651 |
| Amide II (CN stretching, NH bending) | 1480–1575 |
| Amide III (CN stretching, NH bending) | 1229–1301 |
| Amide IV (OCN bending) | 625–767 |
| Amide V (Out-of-plane NH bending) | 640–800 |
| Amide VI (Out-of-plane C=O bending) | 537–606 |
| Amide VII (skeletal torsion) | 200 |

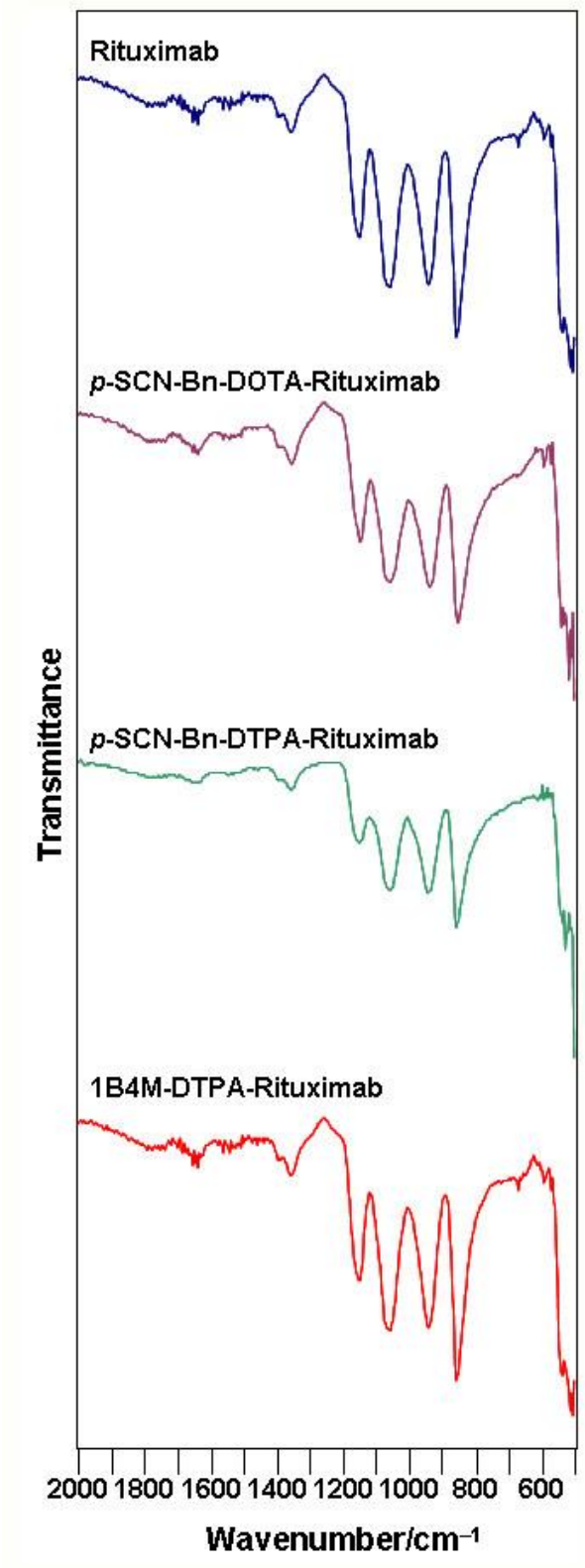


**Fig. 2.** ATR-IR spectra of rituximab, *p*-SCN-Bn-DOTA-rituximab, *p*-SCN-Bn-DTPA-rituximab and 1B4M-DTPA-rituximab (unlabeled and lyophilized)

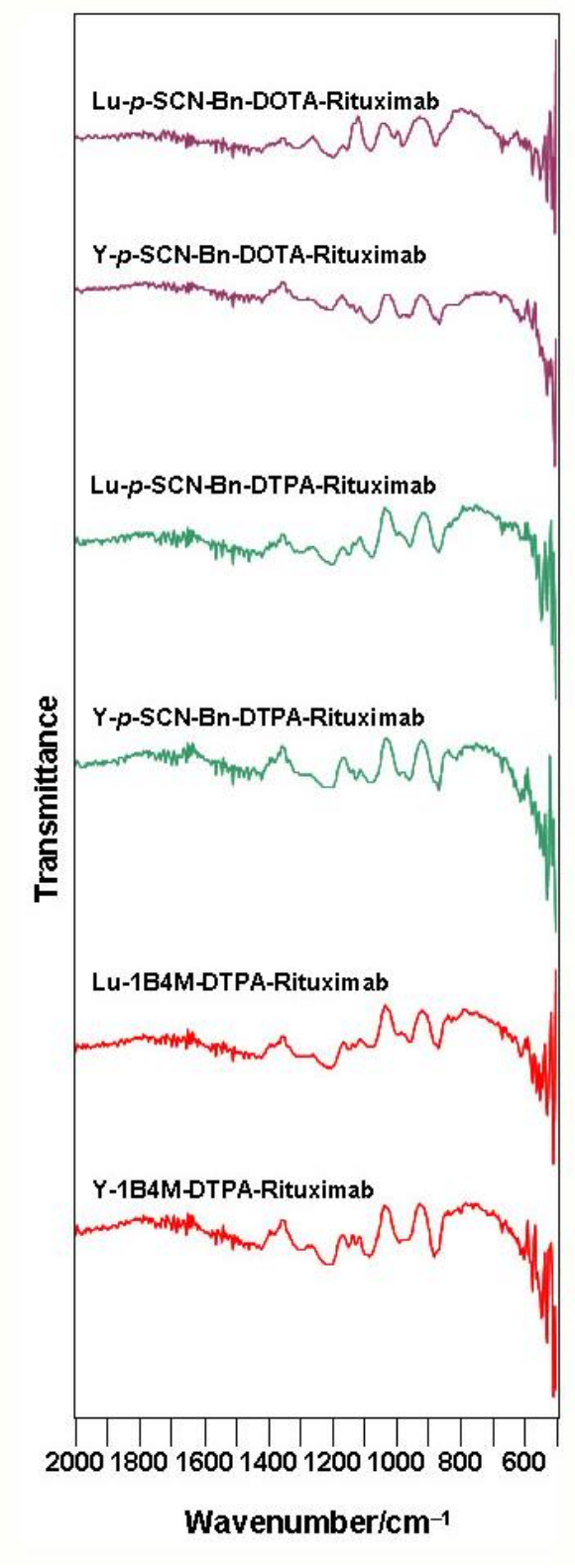


**Fig. 3.** ATR-IR spectra of three types of BFCA-rituximab conjugates labeled with non-radioactive Lu or Y

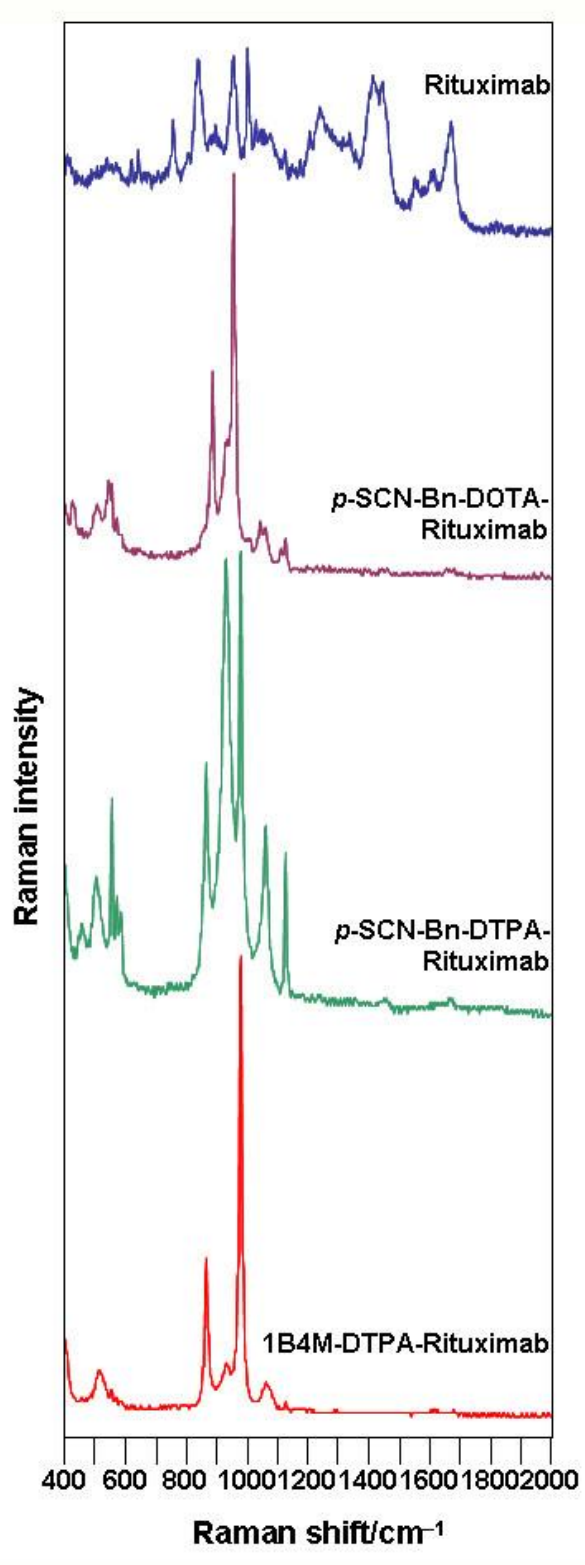


**Fig. 4.** Raman spectra of rituximab, *p*-SCN-Bn-DOTA-rituximab, *p*-SCN-Bn-DTPA-rituximab and 1B4M-DTPA-rituximab (unlabeled and lyophilized)

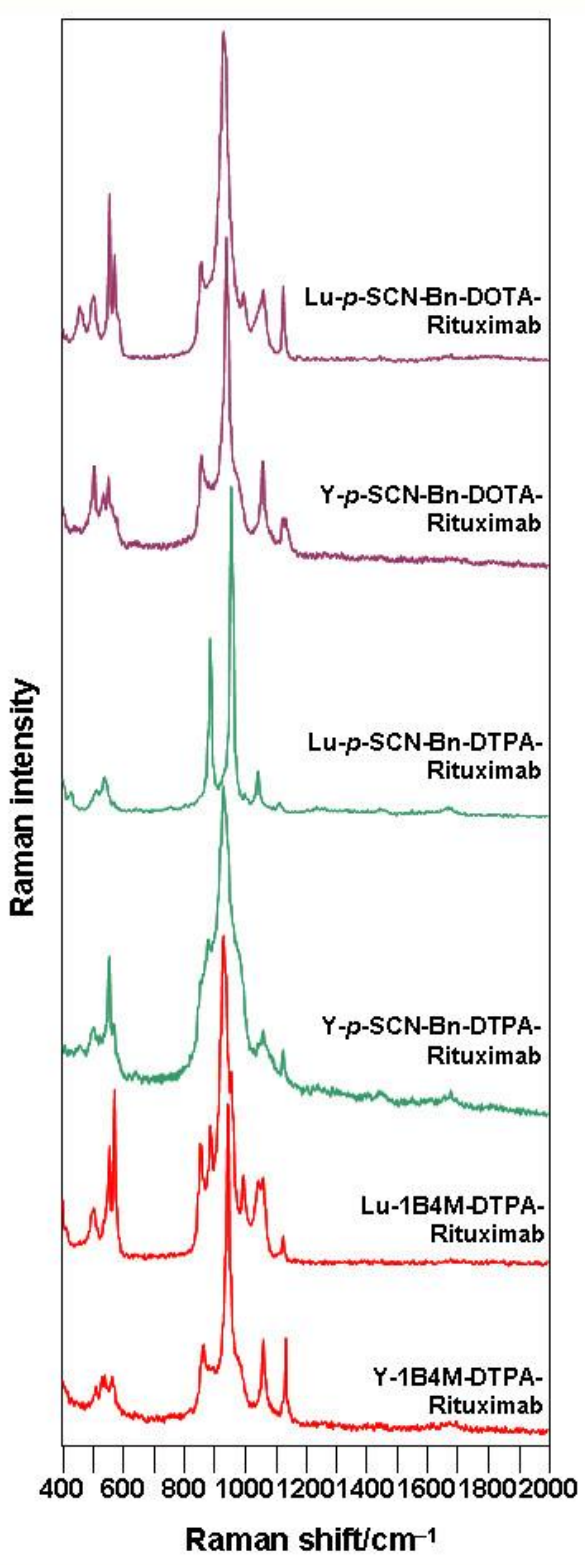


**Fig. 5.** Raman spectra of three types of BFCA-rituximab conjugates labeled with non-radioactive Lu or Y

Table 2

*Assignments of IR bands ($cm^{-1}$) characteristic for the investigated rituximab immunoconjugates (labeled and unlabeled)*

| | Assignments | | | | |
|---|---|---|---|---|---|
| **Sample** | **Amide VI** | **Amide IV and Amide V** | **Amide III** | **Amide II** | **Amide I** |
| **Rituximab** | 537m[a]; 545sh; 571w; 584w; 591w | 627w; 636w; 647w; 671m | 1235w | 1459w; (1510w)[b]; (1540m); 1561m | (1620w); 1636w; (1647w); 1655m; (1688w) |
| ***p*-SCN-Bn-DOTA-rituximab** | 538m; 570m; 585sh; 591m | 670vw | 1351s | 1475vw; (1507w);1562w | (1638m); (1656m); 1678w |
| **Lu-*p*-SCN-Bn-DOTA-rituximab** | 537m; 551s; 572m; 592m | 628w; 651vw; 670m; 690w; 718w; 735w; 758w | 1315vw | 1472m; 1490m; (1508m); (1543m); 1558m; 1575m | (1620w); 1640w; (1647w); (1656w); 1673m; (1684m) |
| **Y-*p*-SCN-Bn-DOTA-rituximab** | 551s; 561sh; 572s; 591w; 606m | 671m; 700w; 720w; 741w; 775w | 1215vw | 1456m; 1472w; 1490w; (1508m);(1541m); 1560m | (1620w); 1636m; (1648w); (1656w); (1684m) |
| ***p*-SCN-Bn-DTPA-rituximab** | 543w; 571w; 576m; 592w | 648vw | 1262vw | (1543w); 1575w | 1636w; (1656w); (1679w) |
| **Lu-*p*-SCN-Bn-DTPA-rituximab** | 546s; 552sh; 563m; 573m; 591w | 636w; 670m; 722w; 742w | 1205m | 1475m; 1490w; (1510w); (1541w); 1561w; 1577w | 1637w; (1656w); 1684w |
| **Y-*p*-SCN-Bn-DTPA-rituximab** | 538sh; 540m; 561m; 573m; 601w | 638m; 648w; 670m; 709w; 728w; 758w; 797w | / | 1474m; 1490m; (1508m); (1542w); 1560w; 1579w | (1620w); 1637w; (1656w); (1684w) |
| **1B4M-DTPA-rituximab** | 538m; 545sh; 584w; 592w | 628vw; 646w; 670m | 1237vw | 1460w; 1474vw; (1508w); (1543w); 1562m; 1577w | 1637m; (1648w); 1655s; 1677w; (1687m) |
| **Lu-1B4M-DTPA-rituximab** | 542m; 551m; 563m; 572m; 592w; 600sh | 635w; 651w; 670m; 742vw | 1205m | 1474w; (1507m); (1545m); 1559w; 1577w | (1620w); 1640w; (1648w); 1655w; 1673w; (1687w); 1699w |
| **Y-1B4M-DTPA-rituximab** | 538sh; 545s; 552sh; 563sh; 572s; 600m | 636w; 643w; 670m; 678w; 713w; 738w; 760w | 1270w | 1475w; 1490w; (1507w); (1542m); 1559m; 1578m | (1620w); 1637w; (1648w); (1686s) |

[a]vw: very weak, w: weak, m: medium, s: strong, vs: very strong, sh: shoulder;
[b]frequencies given in parenthesis matching the literature data [20, 30, 31, 32].

Table 3

*Assignments of Raman bands ($cm^{-1}$) characteristic for unlabeled and non-radioactive labeled-conjugated antibody*

| | Assignments | | | | | | | | | | | | | | |
|---|---|---|---|---|---|---|---|---|---|---|---|---|---|---|---|
| **Sample** | **S-S** | **Tyr** | **Trp** | **Tyr** | **Trp** | **N-Cα-C** | **Trp, Val** | **Phe** | **C-N** | **Amide III** | **Trp, $C_a$-H (def)** | **C-H (def)** | **Indole ring-Trp** | **Tyr, Trp, Phe** | **Amide I** |
| **Rituximab** | 407m[a]; 416m; 529w; (540m)[b] | 623w 640m | 757s | (840s); (854sh) | (878w) | 953sh | (958s); 985w | (1004s); (1012sh); (1031w) | (1123w) | (1245m) | (1337w); 1359w | (1449s) | (1554m) | 1605w; (1614sh) | (1670s) |
| ***p*-SCN-Bn-DOTA -rituximab** | 428m; (505m); (547sh); (555m) | / | / | (857sh) | 886s | (931sh) | (957s) | (1010sh); 1044w; 1060w | 1112sh; (1126m) | / | / | / | (1556vw) | / | (1671vw) |
| **Lu-*p*-SCN-Bn-DOTA-rituximab** | 455m; (505m); 556s; 574sh | / | / | (860m) | / | (937s) | 990m | (1002w); 1062s | (1128m); 1174vw | / | 1390vw | / | / | / | (1666vw) |
| **Y-*p*-SCN-Bn-DOTA -rituximab** | 402s; (505m); (540m); (553m); 584w | / | / | (859m) | / | (942s) | 970sh | 1065m | (1128w) | / | / | / | / | / | (1663vw) |
| ***p*-SCN-Bn-DTPA-rituximab** | 400m; 458w (505m); 557s; 572m; | / | / | (864s) | / | (929s) | (980s) | 1061s | (1126s) | 1213w | 1355w | (1445vw) | / | / | (1671vw) |
| **Lu-*p*-SCN-Bn-DTPA-rituximab** | 400m; 431w; (505w); (540m); 557sh; 574w | / | / | (861sh) | (885s) | 959s | 982sh | (1002w); 1046m; 1063sh | 1115w | / | / | 1447vw | / | / | (1663vw) |
| **Y-*p*-SCN-Bn-DTPA-rituximab** | 404vw; 503m; 555s; 572m; | / | / | 823vw; (857sh) | 886m | 934s | 982sh | 1060s | (1128m) | / | / | / | / | / | (1675m) |
| **1B4M-DTPA-rituximab** | 400m; 507w; 555w; | / | / | 868s | / | 925sh; (932w) | (978s) | 1063m | (1128w) | / | / | / | / | 1609w | (1671w) |
| **Lu-1B4M-DTPA-rituximab** | 400m; (505m); 556sh; 574m | / | / | (860m) | 888m | (930s) | 961sh; 990m | (1048sh); 1062m | (1132w) | (1270w) | / | / | / | / | (1673w) |
| **Y-1B4M-DTPA-rituximab** | 400m; (505m); (538w); 555w; 565w | / | / | (840sh); (857m) | 886w | (944s) | (978w) | 1063m | (1135m) | 1228w | 1357w | 1406w | 1568vw | / | (1675vw) |

[a]vw: very weak, w: weak, m: medium, s: strong, vs: very strong, sh: shoulder;
[b]frequencies given in parenthesis matching the literature data [26, 31, 33, 34, 35].

The correlation between the band frequency and the secondary structure of the protein arises from the fact that the hydrogen bonding between the polypeptide bonds is different in α-helix, β-sheet, or disordered structures [34]. An antibody molecule predominantly consists of *β*-sheet (47%), *α*-helices (7%), and turns and coils (the remaining percentage) [36]. The following three signals are most significant for the identification of different protein backbone confirmations: amide I (stretching vibration of C=O), amide II and amide III (both associated with coupled C–N stretching and N–H bending vibrations of the peptide bond) [37]. Typical β-sheet proteins, as monoclonal antibodies, show a characteristic Amide I band at around 1650–1690 $cm^{-1}$ which is the most sensitive spectral region and consists of overlapping component bands, originating from α-helices, β-sheets, turns and random structures.

Here, we observed that investigated protein components regain their native conformation upon rehydration (reversible unfolding). A strong band in the region between 1612 and 1640 $cm^{-1}$ and a weaker band around 1685 $cm^{-1}$ are commonly observed for β-sheets, although weak bands at lower frequencies (1665–1670 $cm^{-1}$) have also been detected [31]. For all samples, unlabeled and labeled rituximab conjugates, we detected predominantly bands characteristic for β-structure (Tables 2 and 3), which is in accordance with the previously published data [30, 31, 38, 39]. Furthermore, proteins known to adopt α-helical conformation have strong amide I bands between 1650 and 1655 $cm^{-1}$. In all studied samples, bands at 1655 or 1656 $cm^{-1}$ were detected, pointing out that α-helices are present in the structure. The existence of non-ordered (or random) structure is evidenced from the IR band with the centroid around 1645 $cm^{-1}$. In the corresponding spectra of rituximab as well as in the spectra of all *p*-SCN-Bn-DOTA- and 1B4M-DTPA-conjugates, bands at 1647 or 1648 $cm^{-1}$ were detected, which revealed the presence of non-ordered structure in the molecule.

The appearance of a singlet Raman band around 1670 $cm^{-1}$ (Table 3) is explained by the fact that amide I band of turns overlaps and overlays those of α-helices and β-sheets making its assignment difficult. Although the presence of unordered or random structure in the conjugates from the IR spectra is generally assigned according to the band at around 1645 $cm^{-1}$, the corresponding Raman band is blue-shifted to 1665 $cm^{-1}$. The bands appearing at higher frequencies are attributed to the α-helix vibrations in the structure.

According to the previously published data [31], a strong amide II band in the IR spectra of proteins is observed in the 1540–1550 $cm^{-1}$ region accompanied by a weaker shoulder at 1510–1525 $cm^{-1}$. Components with an antiparallel β-sheet structure exhibit strong amide II bands between 1510 and 1530 $cm^{-1}$, whereas somewhat higher frequencies (1530–1550 $cm^{-1}$) point to the parallel β-sheet structure. Indeed, in the 1507–1510 $cm^{-1}$ region, we detected the bands attributed to the antiparallel β-sheet structure whereas the bands registered around 1540 $cm^{-1}$ unveil the parallel β-sheet structure. In corresponding Raman spectra, bands are overlapped with the bands of other side chain groups (aromatic amino acids) (Table 3).

The amide II and amide III bands, when used in combination with the amide I band, may help to assign the protein structure enabling a more accurate estimation of the helix and the random components (Amide II), as well as a distinction between β and disordered structures (Amide III) [31]. Generally, based on the band frequencies obtained for amide I, II and III bands, the studied compounds contain a higher percentage of β-sheet conformation (antiparallel and parallel) in the structure, followed by α-helices.

The weak intensity of the IR amide III band is due to its occurrence in a region where other mixed vibrations (CH bending, tyrosine and phenylalanine ring vibrations) appear. Bearing in mind the weaker intensity of the Raman bands ascribed to the latter vibrations, the corresponding amide III band is much more pronounced in the Raman spectra (see Table 3).

In addition to characterization of the amide bands, Raman spectroscopy enables the detection and assignment of numerous bands from the amino acid groups. Marker bands of aromatics in proteins are relatively strong and well recognized, but under some circumstances, they can be overlapped with bands of amides and other side chain groups [26]. For example, a typical protein exhibits about 30 Raman bands in the region between 2000 and 400 $cm^{-1}$ and additional bands in the 4000–2500 $cm^{-1}$ interval that are due to the vibrational modes of localized groups such as -NH, -OH, $-CH_3$, $-CH_2$, and -SH [26, 34, 40]. Still, the best defined Raman bands in the protein aromatics are those arising from phenylalanine (Phe), tryptophan (Trp) and tyrosine (Tyr) (Table 3). The majority of proteins, antibodies among them, contain either free sulfhydryls (–C–SH or R–SH) or disulfide groups (or both) [26]. The appearance of the disulfide bonds in the Raman spectra in the low frequency region

between 700 and 400 $cm^{-1}$ was also detected (see Fig. 4, Fig. 5 and Table 3).

The unfolding and misfolding of proteins is an important issue in retaining pharmaceutical stability and the activity of proteins. Denaturation of the native structure, misfolding and subsequent aggregation regularly include a change in the secondary structure. The aggregation of proteins is a problem with serious pharmaceutical/medical implications and therefore, vibrational spectroscopy techniques are valuable for studying the aggregation processes of a wide range of proteins. The thermally-induced aggregation processes of the majority of proteins studied by FT-IR and Raman spectroscopy can be described with a two-state model: the predominant secondary structural element (α-helix or β-sheet) decreases as a function of temperature and is concomitantly replaced by intermolecular aggregates [26, 32].

The appearance of strong absorption bands below 1620 $cm^{-1}$ can be correlated with aggregation, which is usually associated with the formation of strong beta-sheet structures [41]. It is worth mentioning that we observed the retention of the native structure of the antibody and no obvious aggregation (the lowest band frequency detected was 1620 $cm^{-1}$ with weak intensity) (Table 2, Fig. 2 and Fig. 3) occurred in the samples according to the obtained spectra of all labeled and unlabeled conjugates after lyophilization.

However, as shown in Figures 2–5, depending of the chelator type of immunoconjugate, frequency shifts for some of the characteristic bands occurred in the recorded spectra, but it is clear that the chelating agents used do not provoke significant changes in the secondary structure of the antibody. Namely, the immunoconjugate spectra showed peak shifts and intensity variations that could be attributed to conformational changes that occur during conjugation and labeling. Several key spectral areas can be identified, which is consistent with the fact that specific amino acids are shielded from undergoing conjugate formation, while some new amino acid residues are made visible in the spectrum of the immunoconjugates. This is evidenced by the band loss or decrease in band number in the spectral region of aromatic amino acids (Trp and Tyr) in conjugate spectra (labeled and unlabeled), compared to rituximab spectra (Table 3), and could be a result of conformational binding. In the immunoconjugates formed, a decrease in tryptophan residues at 757, 878 and 1337 $cm^{-1}$ was noted.

Upon formation of the immunoconjugates (labeled and unlabeled), the most noted Raman peak shift occurred between 540–400 $cm^{-1}$, which can be attributed to conformational changes through vibrations of the disulfide bonds. In the Amide III region, a peak shift (in IR) or loss (in Raman spectra) of the immunoconjugate may also correspond to conformational changes. The differences which can be observed in Figures 2–5 suggest that the immunoconjugate formation could result in changes to the conformation after binding, the orientation of bonds, and shifts in the intensity of functional group bands. Additionally, new peaks which are not found in the antibody spectra indicate complex formation.

Based on the frequencies assigned for amide I, II and III bands, the studied compounds contain the highest percentage of β-sheet conformation (antiparallel and parallel) in the structure, followed by α-helices. Significant changes were not observed upon conjugation and freeze-drying procedures.

These results indicate that vibrational spectra can be used to identify binding events and assign the obtained frequencies to a particular event in the structure. In addition, amide bands in the obtained vibrational spectra could be used as an analytical tool which enables a quick and reliable way for screening protein pharmaceuticals during the development of lyophilized formulations.

Vibrational spectroscopic data allow the detection of alterations in protein structural models as well as the rapid assessment of conformational changes resulting from ligand binding, aggregation or macromolecular interactions. Knowing which part(s) of a protein adopt a particular secondary structure is important for deciding whether these protein pharmaceuticals meet the given criteria and is critical for almost all protein-modeling approaches.

In summary, we investigated the potential application of vibrational spectroscopy in the assessment of conformational changes during stress conditions, such as lyophilization and non-radioactive labeling, using rituximab as a model antibody. We obtained IR and Raman spectra of the immunoconjugates that are somewhat different from those of the parent antibody. Peak shifts and intensity variations observed could be attributed to conformational changes that occur during conjugation and labeling and it is possible to assign these changes to complex formation. These results provide a good foundation for further radiolabeling studies of the kit formulations for possible therapeutic applications.

***Acknowledgments.*** This work was supported by the IAEA Coordinated Research Project (CRP): Therapeutic radiopharmaceuticals based on $^{177}Lu$ and $^{90}Y$

labeled monoclonal antibodies and peptides: Development and preclinical evaluations.

## REFERENCES


[1] A. Hagenbeek, V. Lewington, Report of a European Consensus 1. Workshop to develop recommendations for the optimal use of $^{90}$Y-Ibritumomab tiuxetan (Zevalin) in lymphoma, *Ann. Oncol.*, **16**, 786–792 (2005).

[2] R. O. Dillman, Monoclonal antibody therapy for lymphoma, *Cancer Pract.*, **9**, 71–80 (2001).

[3] R. O. Dillman, Magic bullets at last! Finally – approval of a monoclonal antibody for the treatment of cancer!!! *Cancer Biother. Radiopharm*., **12**, 223–225 (1997).

[4] R. O. Dillman, Treatment of low-grade B-cell lymphoma with the monoclonal antibody rituximab, *Semin. Oncol*., **30**, 434–447 (2003).

[5] R. O. Dillman, Radiolabeled anti-CD20 monoclonal antibodies for the treatment of B-cell lymphoma, *J. Clin. Oncol*., **20**, 3545–3557 (2002).

[6] B. D. Cheson, Radioimmunotherapy of non-Hodgkin's lymphoma, *Blood*, **101**, 391–398 (2003).

[7] C. R. Dias, S. Jeger, J. A. Jr. Osso, C. Müller, C. De Pasquale, A. Hohn, R. Waibel, R. Schibli, Radiolabeling of rituximab with $^{188}$Re and $^{99m}$Tc using the tricarbonyl technology, *Nucl. Med. Biol.*, **38**, 19–28 (2011).

[8] S. Liu, Bifunctional coupling agents for radiolabeling of biomolecules and target-specific delivery of metallic radionuclides, *Adv. Drug Deliv. Rev*., **60**, 1347–1370 (2008).

[9] S. Liu, The role of coordination chemistry in the development of target-specific radiopharmaceuticals, *Chem. Soc. Rev*., **33**, 445–461 (2004).

[10] P. Thakral, S. Singla, M. P. Yadav, A. Vasisht, A. Sharma, S. K. Gupta, C. S. Bal, A. Malhotra, An approach for conjugation of $^{177}$Lu-DOTA-SCN-Rituximab (BioSim) & its evaluation for radioimmunotherapy of relapsed & refractory B-cell non Hodgkins lymphoma patients, *Indian J. Med. Res*., **139**, 544–554 (2014).

[11] H. Mohsin, J. Fitzsimmons, T. Shelton, T. J. Hoffman, C. S. Cutler, M. R. Lewis, P. S. Athey, G. Gulyas, G. E. Kiefer, R. K. Frank, J. Simon, S. Z. Lever, S. S. Jurisson, Preparation and biological evaluation of $^{111}$In, $^{177}$Lu and $^{90}$Y labeled DOTA analogues conjugated to B72.3, *Nucl. Med. Biol*., **34**, 493–502 (2007).

[12] A. T. Yordanov, M. Hens, C. Pegram, D. D. Bigner, M. R. Zalutsky, Antitenascin antibody 81C6 armed with $^{177}$Lu: in vivo comparison of macrocyclic and acyclic ligands, *Nucl. Med. Biol*., **34**, 173–183 (2007).

[13] S. Rasaneh, H. Rajabi, M. H. Babaei, F. J. Daha, Toxicity of trastuzumab labeled $^{177}$Lu on MCF7 and SKBr3 cell lines, *Appl. Radiat. Isot.*, **68**, 1964–1966 (2010).

[14] M. Hens, G. Vaidyanathan, P. Welsh, M. R. Zalutsky, Labeling internalizing anti-epidermal growth factor receptor variant III monoclonal antibody with $^{177}$Lu: *in vitro* comparison of acyclic and macrocyclic ligands, *Nucl. Med. Biol*., **36**, 117–128 (2009).

[15] J. Hoffend, W. Mier, J. Schuhmacher, K. Schmidt, A. Dimitrakopoulou-Strauss, L. G. Strauss, E. R. M. Kinscherf, U. Haberkorna, Gallium-68-DOTA-albumin as a PET blood-pool marker: experimental evaluation in vivo, *Nucl. Med. Biol*., **32**, 287–292 (2005).

[16] M. R. McDevitt, D. Ma, J. Simon, K. Frank, D. A. Scheinberg, Design and synthesis of $^{225}$Ac radioimmunopharmaceuticals, *Appl. Radiat. Isot.*, **57**, 841–847 (2002).

[17] C. J. Smith, H. Galib, G. L. Sieckmanc, D. L. Hayes, N. K. Owen, D. J. Mazuru, W. A. Volkert, T. J. Hoffman, Gastrin releasing peptide (GRP) receptor targeted radiopharmaceuticals: a concise update, *Nucl. Med. Biol*., **30**, 101–109 (2003).

[18] L. L. Chappell, E. Dadachova, D. E. Milenic, K. Garmestani, C. Wu, M. W. Brechbiel, Synthesis, characterization, and evaluation of a novel bifunctional chelating agent for the lead isotopes $^{203}$Pb and $^{212}$Pb, *Nucl. Med. Biol*., **27**, 93–100 (2000).

[19] J. L. Cleland, M. F. Powell, S. J. Shire, Development of stabile protein formulations: A close look at protein aggregation, deamidation, and oxidation, *Crit. Rev. Ther. Drug Carrier Syst*., **10**, 307–377 (1993).

[20] M. Paul, V. Vieillard, E. Jaccoulet, A. Astier, Long-term stability of diluted solutions of the monoclonal antibody rituximab, *Int. J. Pharm*., **436**, 282–290 (2012).

[21] A. Bhambhani, J. T. Blue, Lyophilization strategies for development of a high-concentration monoclonal antibody formulation: benefits and pitfalls, *Am. Pharm. Rev*., **13**, 31–38 (2010).

[22] J. Park, K. Nagapudi, C. Vergara, R. Ramachander, J. S. Laurence, S. Krishnan, Effect of pH and Excipients on Structure, Dynamics, and Long-Term Stability of a Model IgG1 Monoclonal Antibody upon Freeze-Drying, *Pharm. Res*., **30**, 968–984 (2013).

[23] M. Rankl, T. Ruckstuhl, M. Rabe, G. R. J. Artus, A. Walser, S. Seeger, Conformational reorientation of immunoglobulin G during nonspecific interaction with surfaces, *Chem. Phys. Chem.*, **7**, 837–846 (2006).

[24] B. M. Murphy, N. Zhang, R. W. Payne, J. M. Davis, A. M. Abdul-Fattah, J. E. Matsuura, A. C. Herman, M. C. Manning, Structure, stability, and mobility of a lyophilized IgG1 monoclonal antibody as determined using second-derivative infrared spectroscopy, *J. Pharm. Sci*., **101**, 81–91 (2012).

[25] D. M. Bunk, M. J. Welch, Electrospray ionization mass spectrometry for the quantitation of albumin in human serum, *J. Am. Soc. Mass Spectrom*., **8**, 1247–1254 (1997).

[26] Z-Q. Wen, Raman spectroscopy of protein pharmaceuticals, *J. Pharm. Sci*., **96**, 2861–2878 (2007).

[27] S. Krimm, J. Bandekar, Vibrational spectroscopy and conformation of peptides, polypeptides, and proteins, *Adv. Protein Chem*., **38**, 181–364 (1986).

[28] R. W. William, Protein secondary structure analysis using Raman Amide I and Amide III spectra, *Method Enzymol*., **130**, 311–331 (1986).

[29] J. Banker, Amide modes and protein conformation, *Biochim. Biophys. Acta*, **1120**, 123−143 (1992).

[30] J. Kong, S. Yu, Fourier Transform Infrared Spectroscopic Analysis of Protein Secondary Structures, *Acta Biochim. Biophys. Sin*., **39**, 549–559 (2007).

[31] J. T. Pelton, L. R. McLean, Spectroscopic methods for analysis of protein secondary structure, *Anal. Biochem*., **277**, 167–176 (2000).

[32] A. Dong, T. W. Randolph, J. F. Carpenter, Entrapping intermediates of thermal aggregation in α-helical proteins with low concentration of guanidine hydrochloride, *J. Biol. Chem*., **275**, 27689−27693 (2000).

[33] R. P. Kengne-Momo, P. Daniel, F. Lagarde, Y. L. Jeyachandran, J. F. Pilard, M. J. Durand-Thouand, G. Thouand, Protein interactions investigated by the Raman spectroscopy for biosensor applications, *Int. J. Spectrosc*., **2012**, Article ID 462901, 7 pages (2012).

[34] A. Rygula, K. Majzner, K. M. Marzec, A. Kaczor, M. Pilarczyka, M. Baranska, Raman spectroscopy of proteins: a review, *J. Raman Spectrosc*., **44**, 1061–1076 (2013).

[35] S. Nitahara, M. Maeki, H. Yamaguchi, K. Yamashita, M. Miyazaki, H. Maeda, Three-dimensional Raman spectroscopic imaging of protein crystals deposited on a nanodroplet, *Analyst*, **137**, 5730–5735 (2012).

[36] M. Marquart, J. Deisenhofer, R. Huber, Crystallographic refinement and atomic models of the intact immunoglobulin molecule Kol and its antigen-binding fragment at 3.0 $\theta$ and 1.9 $\theta$ resolution, *J. Mol. Biol*., **141**, 369–391 (1980).

[37] H. Schulz, M. Baranska, Identification and quantification of valuable plant substances by IR and Raman spectroscopy, *Vib. Spectrosc*., **43**, 13–25 (2007).

[38] G. Reiter, N. Hassler, V. Weber, D. Falkenhagen, U. P. Fringeli, In situ FTIR ATR spectroscopic study of the interaction of immobilized human tumor necrosis factor-a with a monoclonal antibody in aqueous environment, *Biochim. Biophys. Acta*, **1699**, 253–261 (2004).

[39] S. U. Sane, R. Wong, C. C. Hsu, Raman spectroscopic characterization of drying-induced structural changes in a therapeutic antibody: Correlating structural changes with long-term stability, *J. Pharm. Sci*., **93**, 1005–1018, (2004).

[40] R. Tuma, Raman spectroscopy of proteins: from peptides to large assembles, *J. Raman Spectrosc*., **36**, 307–319 (2005).

[41] S. Schüle, W. Frieß, K. Bechtold-Peters, P. Garidel, Conformational analysis of protein secondary structure during spray-drying of antibody/mannitol formulations, *Eur. J. Pharm. Biopharm*., **65**, 1–9 (2007).